

The LBT Facility SCIDAR: Recent Results

Daniel L. McKenna ^a, Remy Avila ^b, John M. Hill ^c, Stefan Hippler ^d, Piero Salinari ^e, Paul Stanton ^f, Robert Weiss ^g

^aUniversity of Arizona, Steward Observatory Engineering and Technical Services,
Steward Observatory 933 N. Cherry Av. Tucson , Arizona 85721

^bInstituto de Astronomia UNAM Campus Morelia A.P. 72-3 (xangari) 58089 Morelia Michoacan Mexico

^cUniversity of Arizona Large Binocular Telescope Project, 933 N Cherry Av. Tucson Az 85721

^dMax-Planck-Institut fuer Astronomie, Koenigstuhl 17 D-69117 Heidelberg, Germany

^eOsservatorio Astrofisico di Arcetri, Largo E. Fermi 5, 50125 Firenze, Italy

^f Alacron Inc., 71 Spit Brook Road, Suite, 200 Nashua, NH 03060

^g Max-Planck-Institut fuer Astronomie, Koenigstuhl 17 D-69117 Heidelberg, Germany

Abstract

We present the design and recent results from the Large Binocular Telescope (LBT) facility SCIDAR. To our knowledge, this work is the first SCIDAR designed as a user instrument for routine seeing measurements in support of telescope operations. Using a commercial off-the-shelf approach, we have minimized the resources required for system construction.

Key Words: SCIDAR, adaptive optics, scintillation, seeing

1. Introduction

The Large Binocular Telescope project (LBT) now in the telescope construction phase, will utilize adaptive secondary mirrors as the basis for an IR-optimized system [1]. By combining the beams from the two primaries, interferometry will be possible without the need to track the fringes at a sidereal rate [2]. This arrangement will provide an ideal platform to develop multi-conjugate adaptive optics. To complement the development and operation of this and other systems, a facility SCIDAR project is currently under way at Steward Observatory.

2. SCIDAR (Scintillation Detection And Ranging)

The development of SCIDAR is chronicled in Rocca 74 [3] and Vernin 82 [4]. The extension of the technique to include low level turbulence, known as the generalized mode, is described in Fuchs 95 [5]. An excellent account of SCIDAR theory and application is presented by Avilia 98 [6]. The SCIDAR technique utilizes moving scintillation patterns from a single or double star. The generalized SCIDAR measures scintillation from the level of the primary mirror by moving the detector from the pupil position to a distance that is optically equivalent to about 3 to 4 km behind the pupil plane. Figure (5) is a generalized pupil image of a double star taken with a 1.8 m telescope. The motion and evolution of the scintillation requires that the pattern be sampled every 10 to 20 milliseconds with an exposure time of 1 millisecond. The combination of the short exposure times with the low light levels unfortunately requires the use of image intensification. The image intensifier, while expensive and delicate, does solve the short exposure time problem without using mechanical shutters. As described in the above SCIDAR references, spatial autocorrelation and spatio-temporal cross correlation of successive scintillation frames provides information on turbulence strength and velocity as a function of altitude and time.

Figure (6) is an example of an auto-correlation image produced by a generalized SCIDAR. The image consists of a central spot at pixel (128,128) and a set of three spots on each side. The two small spots on each side of center are the 4km scintillation at the level of the primary mirror and dome. The 4km height is due to the generalized mode and is set by the observer. The outer set is produced by turbulence at an altitude of 13km. Figure (7) shows the cross-correlation image of the data used in Figure (6). Figure (8) is the negative image of Figure (7). Figures (7,8) illustrates how the lagged cross-correlation image reveals the velocity by the displacement of the SCIDAR triplet, while altitude, is indicated by the separation of the outside spots. Figures (7,8) also demonstrate the smearing effect of wind shear on the cross-correlation image. In addition to the velocity dispersion, Figures (7,8) also illustrate that the intrinsic spot size in both the auto and cross-correlation is due to the Fresnel scale which scales as the square root of the distance to the turbulent layer. Weakly visible in Figures (7,8) is scintillation at a lower altitude than the 13 km layer but with 3 times the velocity. The velocity scale of Figures (7,8) is 0.28 m/s per pixel, thus the weak layer has a velocity across the pupil of 18 m/s and the high layer 6 m/s. It is not unusual to observe the highest altitude layers (13-20 km) moving with a lower velocity than the midlevel turbulence in the summer months. The example in Figure (9) shows the type of complex structure commonly observed in the wintertime when the jet stream is near. In Figure (10) a strong ground layer is present with a high altitude layer.

3. Goals of the LBT SCIDAR project

- 1) Development of an off-the-shelf, real-time SCIDAR instrument
- 2) Collection of turbulence profiles at different sites
- 3) Collection of local and web-based meteorological data for correlation with SCIDAR data
- 4) Production of turbulence models required for adaptive optics and related engineering studies
- 5) Testing of models and algorithms to predict turbulence and its subsequent optical impact
- 6) Optimization of SCIDAR in the observing environment

4. The off-the-shelf SCIDAR

4.1. Optical bench and collimator

Figure (2) is the current SCIDAR mounted on the VATT 1.8-meter telescope located on Mt Graham, Arizona. The enclosure is constructed around a 1-meter optical bench. Figure (3) shows a zoom lens used as a collimator so that a range of F-ratios and pupil diameters can be accommodated. A 4% beam splitter is used in front of the collimator to direct light to a video CCD guide camera. The camera is mounted on a V-groove (Figure 3) so that during alignment an in-focus star appears when the telescope is focused relative to the collimator. If desired during observation the camera can be moved to a position to view the extra-focal image, making the turbulence induced scintillation pattern visible.

4.2. Image intensifier

The gated image intensifier assembly is manufactured by Stanford Computer Optics [8]. Our configuration uses an extended S20 photo-cathode amplified by a two stage micro channel plate electron multiplier. The image intensifier's P46 phosphor screen is imaged onto the detector with a F/0.8 relay lens. An external one shot gate generator, capable of producing 1.0, 0.1, or 0.01 millisecond pulse widths, is used to gate the image intensifier.

4.3. CCD camera

A Dalsa CA-D1256T camera is used as the detector. The camera has two binning modes: bin-by-1 and bin-by-2, yielding a 256 X 256 or 128 X 128 pixel image. The maximum read rates are 125 FPS and 210 FPS for the bin-by-1 and bin-by-2 modes respectively. The combination of the image intensifier and CCD camera produces an image scale of 50 microns per pixel in the bin-by-1 mode. The mechanical interface between the intensifier and camera is simple as both devices comply to the "C mount" standard. The camera image is transmitted to the image processing system via a 30-meter cable to a location outside of the telescope environment.

4.4. Image acquisition and high speed processing

The goal for a real-time SCIDAR requires us to minimize the processing time for computations of cross and auto-correlation images. We accomplish the task of data acquisition, correlation, and display by using the Alacron Fast Image product series [9]. Software was developed by Alacron that met our requirements for processing, display, and storage. For a typical SCIDAR integration at 100 FPS, the 512MB image buffer stores 5000 frames or 50 seconds of data. The data is processed and written to 3 output files (average, cross-correlation, and auto-correlation) 7 seconds after the last frame of data is acquired. The total cycle time from start to finish is 57 seconds. We feel that this provides satisfactory performance for our requirements. Figures (5,6,7) are examples of the three images produced.

4.5. Post processing

We use the SCAVENGER package developed at MPIA [7] to reduce the correlation functions to C_n^2 turbulence profiles. This package currently runs under IDL and is used manually to process SCIDAR data. The facility SCIDAR processing will be automated so that all parameters are set from an object catalog requiring only the catalog object name to reduce the profiles. As part of the reduction process, a "T matrix" is computed that transforms the radial auto-correlation profile to C_n^2 as a function of altitude above the site. This calculation takes the majority of the processing time and thus could be pre-computed in advance. A current goal for post processing is to complete the reduction in under a minute.

5. Other modes of operation.

The high-speed camera system lends itself to other modes of operation that may be useful in this project. To verify the total integrated optical turbulence as computed in post processing, a lens array placed in the pupil plane converts the SCIDAR to a Shack/Hartmann wave front sensor. Using this as a differential image motion monitor, a second method for the determination of r_0 can be used as a crosscheck.

The lens array can be replaced with a re-imaging lens and used to measure the LBT tracking and servo response relative to the optical axis. In addition, these data will also be useful in vibration measurements.

6. Collection and correlation with meteorology data

During the collection of SCIDAR data, local meteorology data is collected when available. On Mt Graham we are developing ruggedized temperature probes to measure C_t^2 . This data will be used to correlate the low-level turbulence measured with the SCIDAR with the temperature measurements at various locations. Data are collected from various web sites that contain upper air data as well as clear air turbulence predictions for aviation needs. It has been useful to use the READY site[10] for upper air wind and cloud prediction. In addition to testing existing meteorological products [11,12], the long term collection of SCIDAR data will complement the verification of turbulence models based on meso-scale models such as MM5 or Meso-Nh [14].

6.1. High resolution radiosonde data

Radiosondes are released every 12 hours from the nearby Tucson Airport. This data is collected by the National Weather Service and is distributed as a standard data set up to the pressure altitude of 100 mb. Unfortunately the radiosonde data is reduced to about 79 altitude levels and lacks sufficient resolution to predict all optically significant turbulent layers. In addition, the 100mb level (16.5km) is too low an altitude for seeing studies as optically significant turbulence has been observed above 20km. Normally a high-resolution data product with 50-meter or better resolution is currently available only two years after it is collected. We have made arrangements to collect the high-resolution 6-second data from the local National Weather Service office on a more immediate basis, and will use it to calibrate an optical turbulence estimator based on the 6-second radiosonde data. If successful, we will be able to infer the turbulence and seeing climate from the archived profiles enabling us to access the long-term seeing statistics calibrated by our SCIDAR data set

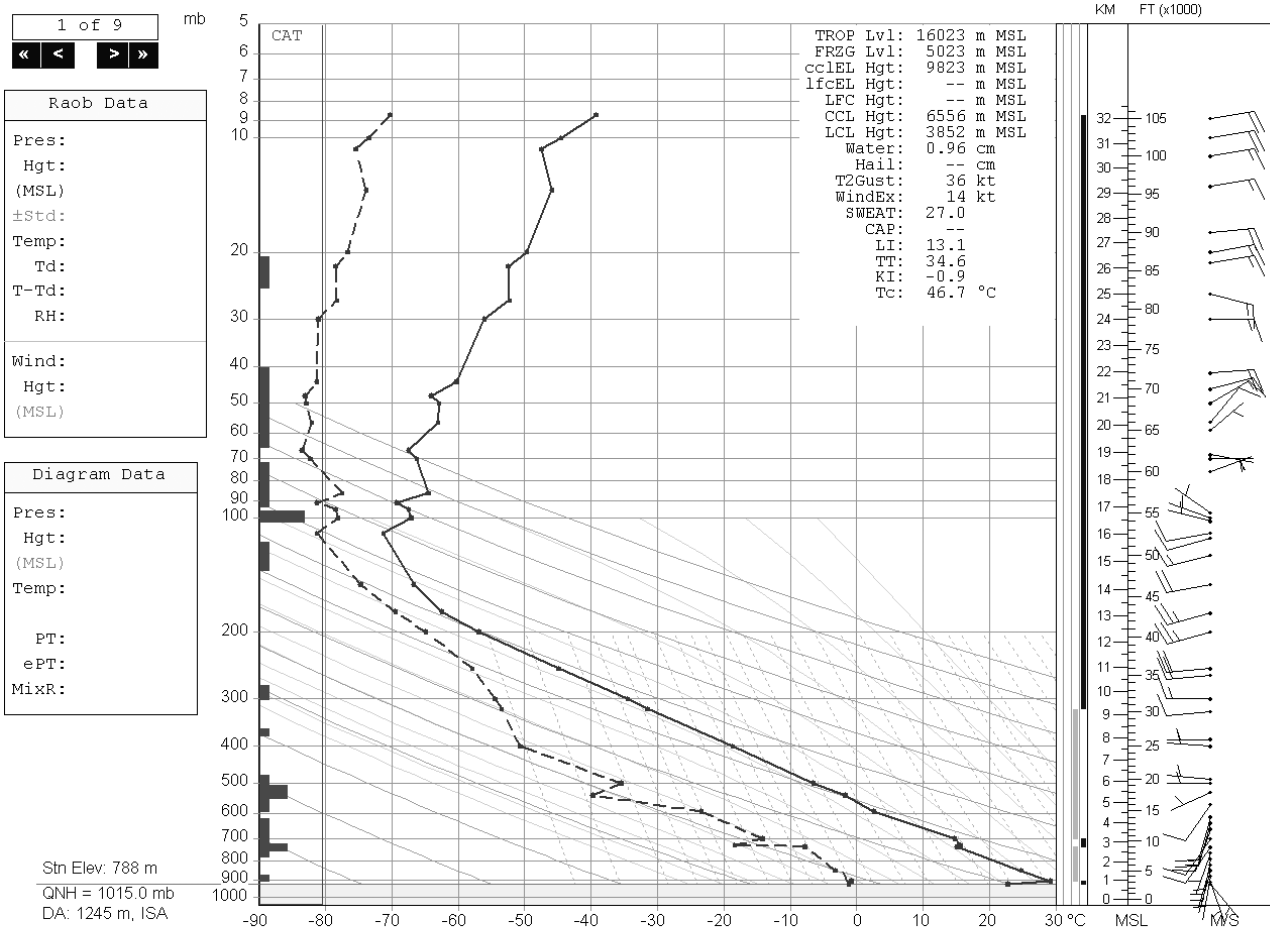


Figure (1) 06/2302 12Z Tucson radiosonde data

The solid line is the air temperature as a function of altitude and the dashed line is the dew point. On the right side of the diagram are wind flags in meters per second, pointing in the direction the wind is coming from. For example, the uppermost wind flag has a velocity of 20 m/s and indicates that the wind is out of the west. Next to the wind scale, the altitude is displayed in km or 1000's of feet. On the left side of the diagram, a display of predicted clear air turbulence is indicated with the length of the bar representing turbulence intensity. The Tropopause is at an altitude of 16km. To the left of the altitude scale, the dark bar indicates stable air and the gray bar is unstable. Optically significant turbulent layers can be found at the boundary between unstable and stable air seen in this diagram at 9.2 km and the inversion at 3 km. The clear air turbulence maximum near 6km also shows up on the SCIDAR data in Figure (4).



Figure (2) LBT SCIDAR instrument on the VATT 1.8meter telescope with the SCIDAR observer shown for scale. The detector position is set to -3.5 km or 157 mm behind the pupil plane.

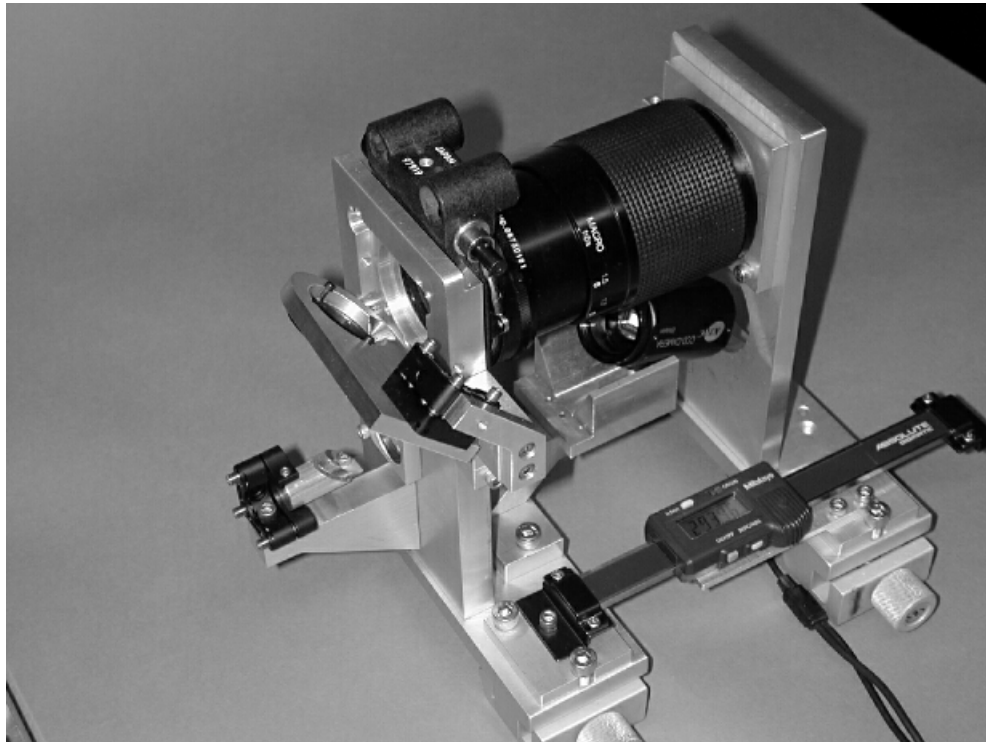


Figure (3) LBT SCIDAR Collimator and guide camera



Figure (4) LBT SCIDAR Image intensifier and guide camera

In Figure (3) the digital micrometer is used to set the focal length of the zoom lens, which changes the pupil diameter projected on the detector. The analysis plane is adjusted by sliding the detector back from the pupil plane.

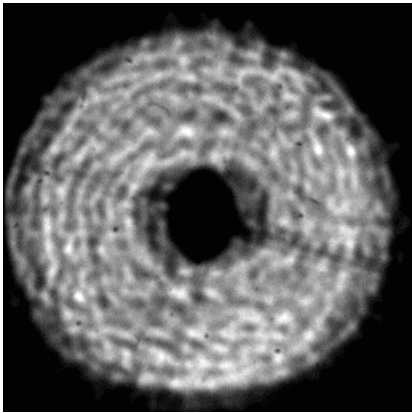


Figure (5) Pupil Image with a double star

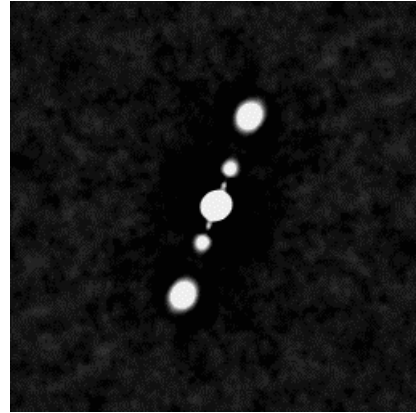


Figure (6) auto-correlation image

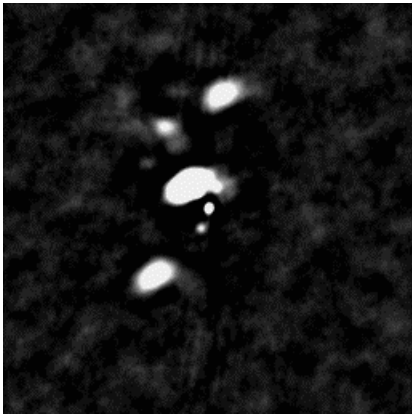


Figure (7) cross-correlation image

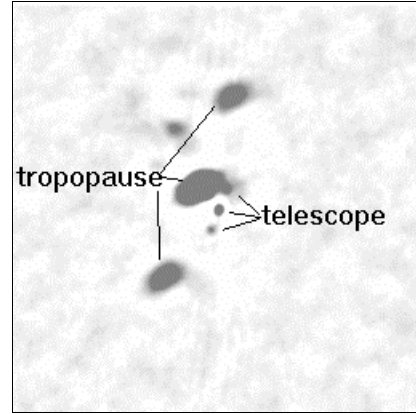


Figure (8) cross-correlation image



Figure (9)



Figure (10)

Figures (9) and (10) exhibit artifacts on the cross-correlation image due to the rotation of the pupil common with ALT/AZ telescopes.

7. Observations

Observations are currently being made at telescope sites in the State of Arizona. Our primary site of interest is the Mt Graham International Observatory, the site of the LBT telescope. Other sites include Mt. Bigelow, Mt. Hopkins, Mt Lemmon, and Kitt Peak. We have observed a few nights at each site and are not yet able to discuss the seasonal statistics associated with these data. For this reason, none of the examples should be considered statistically significant for these sites. Data taken at Mt Graham occurred in the winter season and so the best conditions have not yet been sampled at that site.

7.1. Mt. Hopkins June 19th 2002

Data were obtained during the interval 6/19/2002 through 6/23/ 2002 at the Mt. Hopkins “Ridge” site (alt.2.2km), using the 2MASS 1.3m telescope. The profile obtained on the night of the 23rd has a computed r_0 of 24 cm. at 0.5 microns and a isoplanatic angle of 4.9 arc seconds.

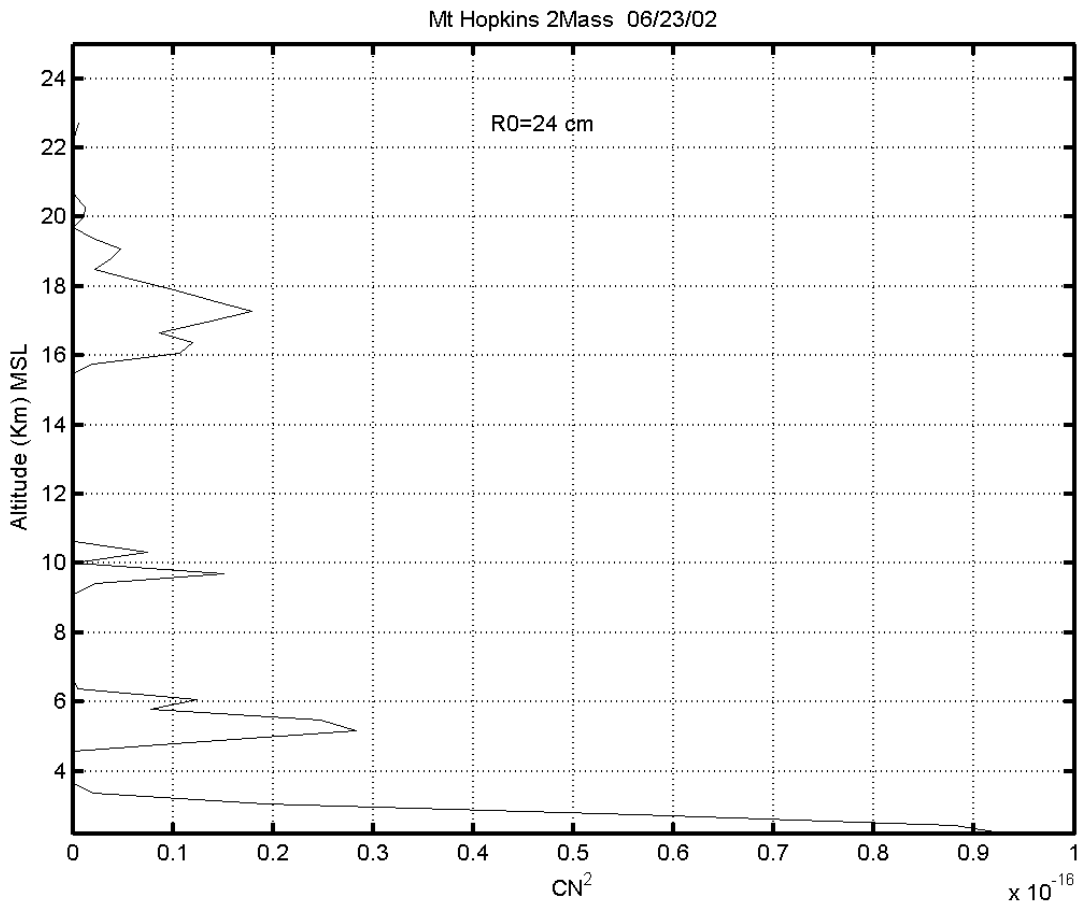


Figure (11)

On this night the telescope /ground layer was the most intense followed by the 5km layer. The 16km layer is at the altitude of the Tropopause and is commonly seen in the SCIDAR data.

7.2. Mt. Graham February 7th 2002

The first profile labeled T +1 minute was obtained on the night 02/07/02. The second profile was obtained 9 minutes later and shows a burst of optical turbulence.

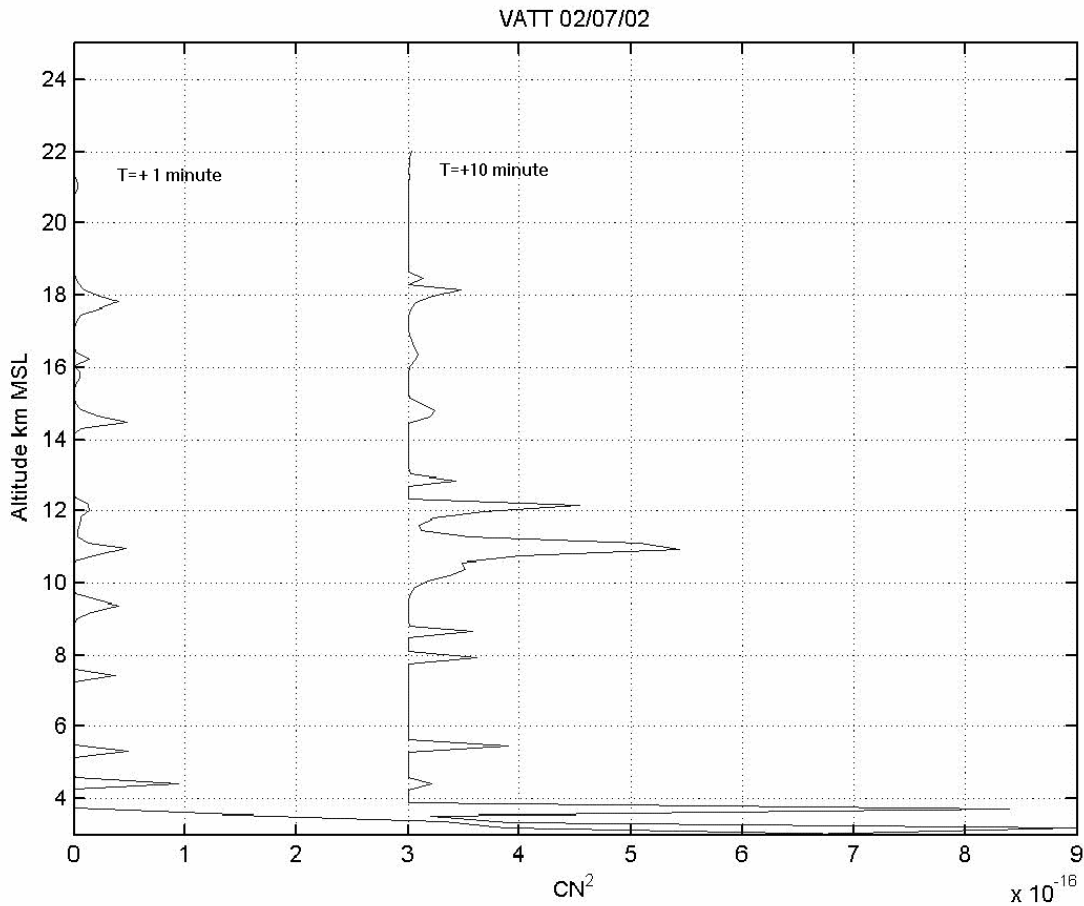


Figure (12) Burst of Optical turbulence at 10.5 km

Figure (12) consists of two profiles 9 minutes apart. The most intense layer above the telescope in the T=+10 image is about 300 to 400 meters above the telescope site, 3.2km, and may be related to the observed transition between unstable and stable air indicated by the 12Z Tucson radiosonde observation in Figure (16). The cross-correlation image in Figure (14) and (15) are related to the SCIDAR profiles of Figure (12) T=+1 and T=10minutes respectively. The T=+1 minute profile is shifted to the right for clarity. In Figure (12) as well as most of the other nights measured, the strongest layer is at the telescope/dome level.

The 8 velocity features in Figure (14) occur near the inversion at 10-11km visible in Figure (16).

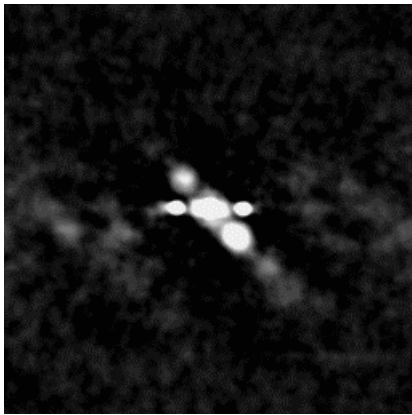
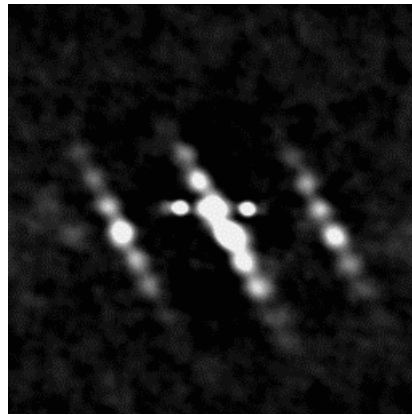


Figure (13) Cross Correlation +1 minute



Figure(14) Cross Correlation +10 minute

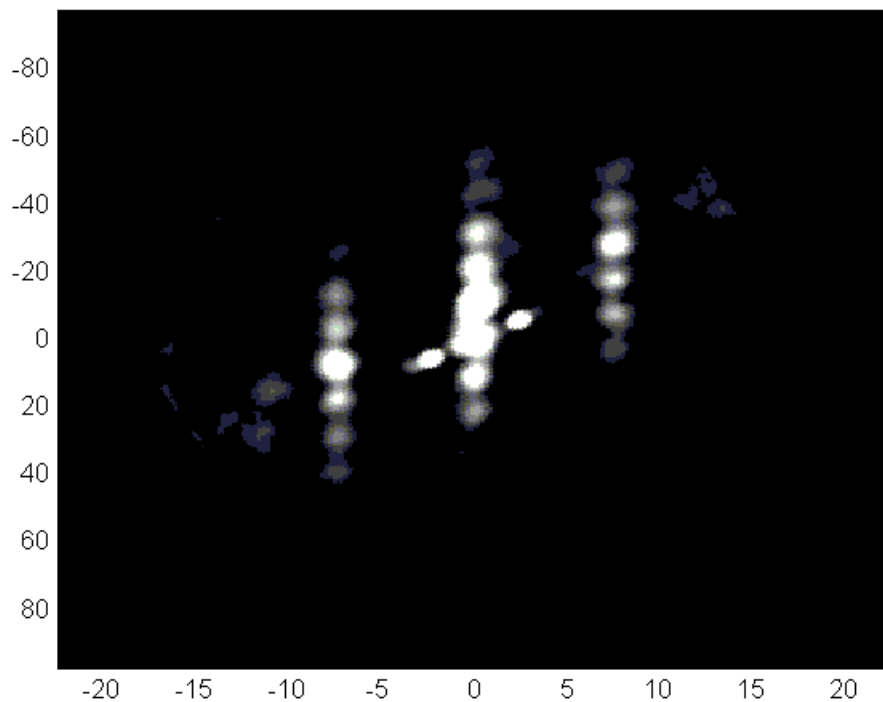


Figure (15) VATT +10 minute Cross Correlation Image Rotated.
The X axis is scaled in km. and the Y in meters/second

The altitude of the turbulence above the telescope can be estimated by the displacement of the SCIDAR triplet from center. This figure illustrates that the turbulent layer has an altitude extent that is not resolved by the SCIDAR. The velocity ranges from -43 m/s to $+30$ m/s. Radiosonde data from Figure (16) indicates a velocity of 22m/s below the layer to 42 m/s above the layer.

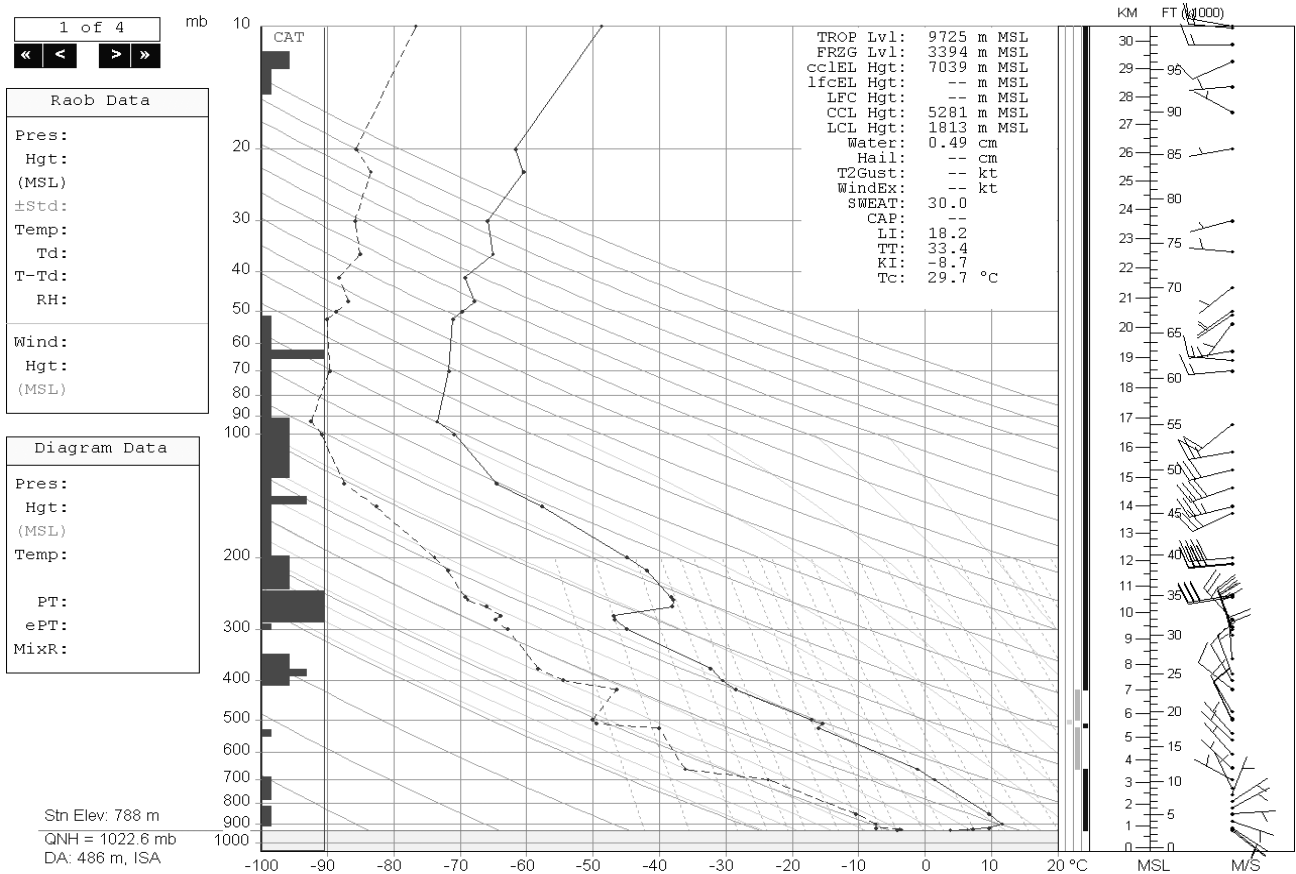


Figure (16) 06/23/02 12 Z. radiosonde Data from Tucson Airport

The radiosonde data reveals an inversion at 5.8 km and a intense inversion at 10.5 km. The wind speed at 9 km. is 22 m/s and at 11 km is 41 m/s. Notice in the Vatt +10 image in Figure (15) that the velocity varies from -30 m/s to +43 m/s. Figure (12) indicates that the velocity features occur at about the same altitude. In this way, the SCIDAR measured velocity data combined with the altitude profile can reveal structure not resolved by altitude but by the velocity dispersion. On the left side of the radiosonde plot is a bar graph of the probability of Clear Air Turbulence (CAT). We have noticed a correlation between CAT Layers as predicted by the RAOB [13] data reduction program used in this study and the altitude of SCIDAR measured optically significant turbulence. This data reveals a case where the radiosonde wind profile underestimates the velocities measured by the SCIDAR. Although we have not yet investigated this case in detail, we suggest that the anomalous velocities in Figure (15) are due to mountain wave breaking, or the related phenomena of lee rotors. Mountain waves, common in complex terrain, have been known to produce persistent atmospheric disturbances. These might induce zones of optically significant turbulence that have a smaller r_0 and a larger velocity dispersion than would be expected from a simple analysis of the upper level winds. The observation of spatially dependent turbulence could be studied using a single star and the velocity signature to map the spatial extent of these regions.

8. Conclusions

We have successfully produced a SCIDAR system using off the shelf components. The SCIDAR is able to operate on various telescopes without changing optics. The goal of real time processing has been met in regards to the high speed processing of the correlation images. We have confidence that our post processing goals will be met in time for the commissioning of the LBT telescope. We emphasize again that the data shown here are examples, and not statistically significant for any of the sites.

We see correlation with the standard radiosonde data set and SCIDAR observations. We will explore using the high-resolution radiosonde data correlated with SCIDAR observations to estimate the turbulence and seeing climatology.

The phenomena of mountain waves may be significant in the production of optically significant turbulence and thus the performance of adaptive optics systems.

The fast camera used in imaging mode will provide a useful tool in the analysis of the LBT tracking and vibration characterization.

9. Reference

- [1] J.M. Hill The Large Binocular Project SPIE Vol. 2871 57 (1996)
- [2] P. Salinari The Large Binocular Telescope Interferometer SPIE Vol. 2871 564 (1996)
- [3] Rocca A., Roddier F., & Vernin J. Detection of atmospheric turbulent layers by spatiotemporal and spatioangular correlation measurements of stellar light scintillation. J. Opt. Soc. Am. 64, 1000 (1974)
- [4] Vernin J. *Atmospheric turbulence profiles* in Wave Propagation in Random Media (Scintillation)-Invited papers SPIE-press and inst. Phys. Publ. 248 (1992)
- [5] Fuchs, A., Tallon, M., & Vernin, J Folding of the vertical atmospheric turbulence profile using an optical technique of movable observing plane in Proc. SPIE on Atmospheric Propagation and Remote Sensing III SPIE 2222, 682 (1994)
- [6] Avila R, (Phd Thesis) These, Caracterisation de la Turbulence Atmospherique pour la Haute Resolution Angulaire en Astronomie: Mise en oeuvre et Exploitation du SCIDAR Generalise et du Grating Scale Monitor (1998)
- [7] Weiss A .R., S. Hippler, Kasper M.E., Wooder N.J., Quartel J.C., Simultaneous Measurement of the Fried Parameter r_0 and the Isoplanatic Angle using SCIDAR and adaptive optics (these proceedings)
- [8] Stanford Computer Optics, Inc. 780 Cragmont Avenue Berkeley, CA 94708 USA Phone:(510)527-3516
- [9] Alacron Inc. 71, Spitbrook Road, suite 200, Nashua, N,H, 03060 (603) 891-2750
- [10] READY www.arl.noaa.gov/ready/cmet.html
- [11] F.S.L. www-frd.fsl.noaa.gov/mab/tke/
- [12] adds.aviationweather.noaa.gov/projects/adds/turbulence/
- [13] Raob 5.1 Environmental Research Services www.raob.com
- [14] Masciadri E., Vernin J, Bougeault P. 3D mapping of optical turbulence using an atmospheric numerical model II. First results at Cerro Paranal Astron. Astrophys. Suppl. Ser. 137, 203-216 (1999)